

Gene Therapy Preserves Retinal Structure and Function in a Mouse Model of *NMNAT1*-Associated Retinal Degeneration

Scott H. Greenwald,¹ Emily E. Brown,^{1,3} Michael J. Scandura,^{1,3} Erin Hennessey,¹ Raymond Farmer,¹ Basil S. Pawlyk,¹ Ru Xiao,^{1,2} Luk H. Vandenberghe,^{1,2} and Eric A. Pierce¹

¹Ocular Genomics Institute, Department of Ophthalmology, Massachusetts Eye and Ear Infirmary, Harvard Medical School, Boston, MA 02114, USA; ²Ocular Genomics Institute, Grousebeck Gene Therapy Center, Department of Ophthalmology, Massachusetts Eye and Ear Infirmary, Harvard Medical School, Boston, MA 02114, USA

No treatment is available for nicotinamide mononucleotide adenylyltransferase 1 (*NMNAT1*)-associated retinal degeneration, an inherited disease that leads to severe vision loss early in life. Although the causative gene, *NMNAT1*, plays an essential role in nuclear nicotinamide adenine dinucleotide (NAD)⁺ metabolism in tissues throughout the body, *NMNAT1*-associated disease is isolated to the retina. Since this condition is recessive, supplementing the retina with a normal copy of *NMNAT1* should protect vulnerable cells from disease progression. We tested this hypothesis in a mouse model that harbors the p.Val9Met mutation in *Nmnat1* and consequently develops a retinal degenerative phenotype that recapitulates key features of the human disease. Gene augmentation therapy, delivered by subretinal injection of adeno-associated virus (AAV) carrying a normal human copy of *NMNAT1*, rescued retinal structure and function. Due to the early-onset profile of the phenotype, a rapidly activating self-complementary AAV was required to initiate transgene expression during the narrow therapeutic window. These data represent the first proof of concept for a therapy to treat patients with *NMNAT1*-associated disease.

INTRODUCTION

Nicotinamide mononucleotide adenylyltransferase 1 (*NMNAT1*)-associated retinal degeneration is an early-onset, recessive disease that causes severe vision loss during the first or second decade of life.^{1–5} The affected gene, *NMNAT1*, encodes a ubiquitously expressed enzyme that is essential for regenerating nicotinamide adenine dinucleotide (NAD)⁺ in cell nuclei.^{1,6} The nuclear NAD⁺ pool is important to many cellular processes, including those related to DNA repair, gene expression, cell signaling, and cell senescence.^{7–10} At least 34 mutations in *NMNAT1* are associated with retinal degeneration,^{10,11} each of which is presumed to decrease enzymatic activity to varying degrees.⁴ Because inheritance of two completely nonfunctional alleles causes embryonic lethality in *Nmnat1* knockout mice, a profound but incomplete loss of nuclear NAD⁺ likely causes disease.¹² While two other *NMNAT* isoforms, *NMNAT2* and *NMNAT3*, have the same NAD⁺ synthase function in the cytosol and in the mitochondria,

respectively,^{8,13} it is apparent that neither can compensate for the loss of *NMNAT1*,¹² at least in the retina. The isolated nature of this disease can be partially explained by the recent finding that neural retinas of *Nmnat1*^{V9M/V9M} mice,¹⁴ the same model used in the present study, have decreased levels of NAD⁺ accompanied by increased levels of an immediate precursor,¹⁵ whereas NAD⁺ levels in other tissues, including brain tissue, remain unchanged (S.H.G., unpublished data). However, the underlying reason that the retina has this unique vulnerability remains unclear.

Currently, no treatment exists for *NMNAT1*-associated retinal degeneration. Because patients incur considerable vision loss during the first years of life, but are expected to have normal longevity, an early intervention has the potential to preserve sight for many decades. Since this disease has a recessive inheritance pattern¹⁰ and because *NMNAT1* is a relatively small gene,¹⁶ treatment with adeno-associated virus (AAV)-mediated gene augmentation therapy is an attractive strategy. At 840 bp, human *NMNAT1* cDNA is well within the ~4.7-kb cargo capacity for single-stranded AAV (SS.AAV)¹⁷ and the ~2.2-kb cargo capacity of self-complementary AAV (SC.AAV).¹⁸ AAV-mediated gene augmentation is presently being used as a US Food and Drug Administration (FDA)-approved therapy for *RPE65*-associated retinal degeneration¹⁹ and in ongoing clinical^{20–23} and pre-clinical^{24–27} trials for other inherited retinal degenerations. In addition, an SC.AAV9-SMN1 vector is approved for the treatment of spinal motor atrophy.²⁸

When *NMNAT1* was reported as a disease gene in 2012,^{1–4} a suitable animal model was not available for evaluating potential therapies *in situ*. Traditional *Nmnat1* knockout mice were not viable,¹² and conditional knockout animals, which have *Nmnat1* ablated in targeted

Received 22 April 2020; accepted 6 July 2020;
<https://doi.org/10.1016/j.omtm.2020.07.003>.

³These authors contributed equally to this work.

Correspondence: Eric A. Pierce, Ocular Genomics Institute, Department of Ophthalmology, Massachusetts Eye and Ear Infirmary, Harvard Medical School, Boston, MA 02114, USA.

E-mail: eric_pierce@meei.harvard.edu



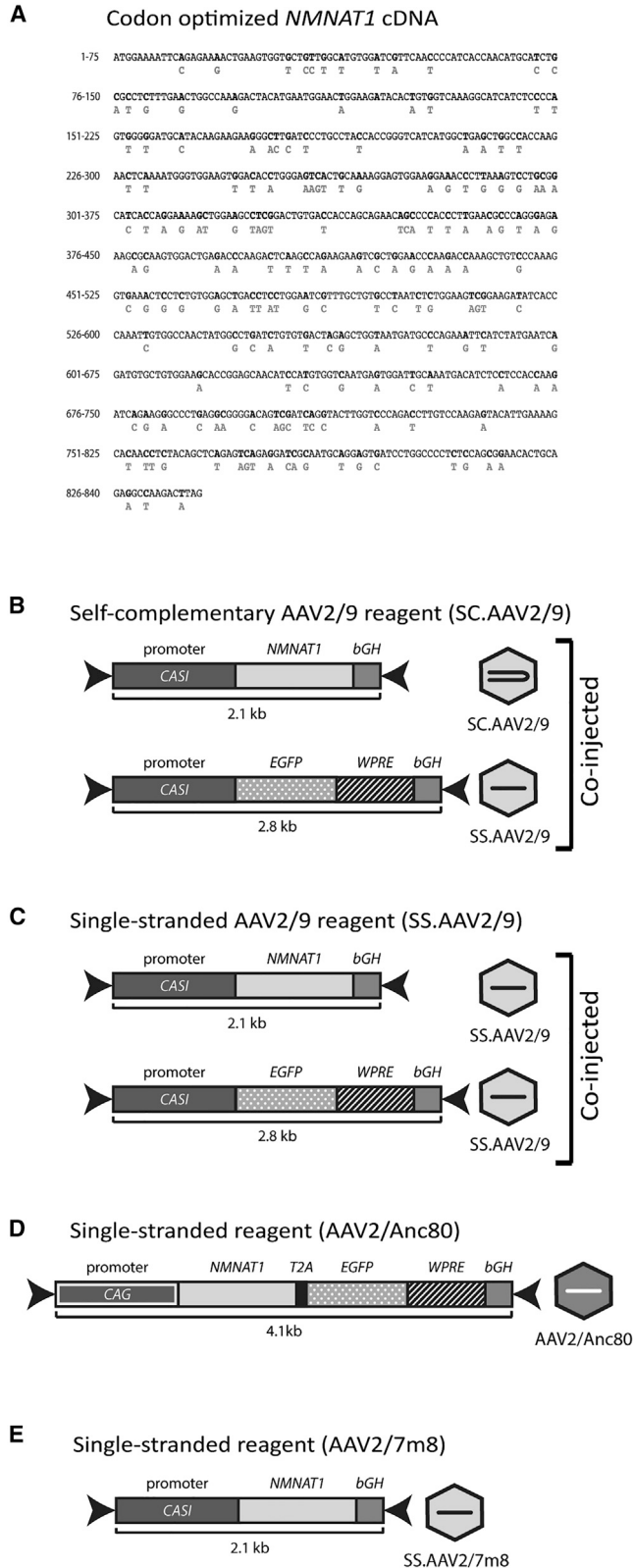


Figure 1. *NMNAT1* Transgene Sequence and Viral Vectors

(A) The 840-nt codon-optimized human *NMNAT1* cDNA sequence has 174 silent substitutions (bold), and the identities of the respective wild-type nucleotides are shown beneath (gray text). (B) *NMNAT1*, driven by the CASI promoter and packaged in the SC.AAV2/9 vector, was co-delivered to mice with an *EGFP* reporter construct that is driven by the same promoter, followed by *WPRE*, and packaged in the SS.AAV2/9 vector. (C) Identical to (B), except that both constructs were packaged in the SS.AAV2/9 vector. (D) A self-cleaving *NMNAT1-EGFP* fusion construct, driven by the CAG promoter and followed by *WPRE*, was packaged in the AAV2/Anc80 vector. (E) *NMNAT1*, driven by the CASI promoter, was packaged into the AAV2/7m8 vector. bGH, bovine growth hormone polyadenylation signal; EGFP, enhanced green fluorescent protein; T2A, *Thomasa signa* virus 2A self-cleaving sequence; *WPRE*, woodchuck hepatitis virus posttranslational regulatory element.

retinal cells, would not have accurately represented the disease physiology. Subsequently, we identified and characterized an *NMNAT1*-associated retinal disease mouse model that is homozygous for the p.Val9Met (V9M) mutation in *Nmnat1*,¹⁴ an allele that has been found to cause retinal disease in members of unrelated families.^{4,10} *Nmnat1*^{V9M/V9M} mice invariably develop an early-onset isolated retinal disease without obvious detriments to longevity or mobility, much like the humans they model. These mice have fully mature retinas and reliable responses to light at 3 weeks of age, as detected by electroretinogram (ERG), but a week later the photoreceptor layer shows signs of degeneration accompanied by reduced function. When the mice reach approximately 4 months of age, the retina is severely degenerated and responses to light stimuli are often undetectable.¹⁴

For the purpose of developing a therapy that preserves vision in people with *NMNAT1*-associated retinal degeneration, we used the *Nmnat1*^{V9M/V9M} mouse model to test the hypothesis that the structure and function of the retina can be rescued if supplemented with normal *NMNAT1*. A human *NMNAT1* cDNA was delivered to the retinas of *Nmnat1*^{V9M/V9M} mice via recombinant AAV vectors that were evaluated independently. Efficacy varied across viral preparations and experimental conditions; therefore, we aimed to understand why specific variables were associated with success or failure and how these lessons might generalize to assist in the development of other AAV-mediated gene therapies.

RESULTS

DNA Construct and AAV Vector Preparation

A codon-optimized human *NMNAT1* cDNA (Figure 1A) was incorporated into constructs that were then packaged into recombinant AAV vectors. Codon optimization has been reported to improve the level and duration of expression of human genes in transduced cells without altering the amino acid sequence of the protein product.^{29–33} All 174 nt substitutions introduced into the 840-bp *NMNAT1* cDNA were silent, defining the normal human protein sequence.

Four DNA constructs and four AAV vector subtypes were used in combination to create vectors that were delivered independently to mice in this study. A construct in which *NMNAT1* was driven by

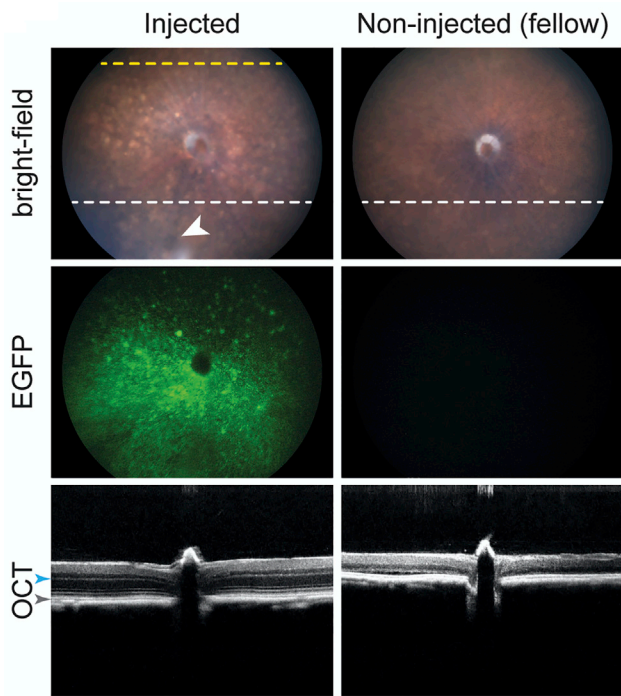


Figure 2. In Vivo Imaging of Injected and Non-injected Retinas

Bright-field fundus image of the injected (left column) and non-injected (right column) fellow retina from a representative 4-month-old *Nmnat1*^{V9M/V9M} mouse treated with the SC.AAV2/9 vector at 2×10^9 gc/ μ L (top row). The superior and inferior planes in which the photoreceptor layer was measured using OCT are marked (yellow and white dashed lines, respectively), as is the injection site (arrowhead) (top row). The EGFP reporter is visible only in fundus image of the injected retina (middle row). Cross-sectional OCT images, acquired at the level of the optic nerve head, show that the injected retina is thicker than the non-injected retina (bottom row). Photoreceptor layer thickness was measured from the outer plexiform layer (blue arrowhead) to the RPE (gray arrowhead).

the ubiquitously expressing CASI promoter was packaged into both a self-complementary and single-stranded version of AAV2/9. The self-complementary vector was selected for testing because it activates gene expression more rapidly than traditional single-stranded vectors.³⁴ A construct containing an *EGFP* (enhanced green fluorescent protein) reporter gene, also driven by the CASI promoter and followed by the woodchuck hepatitis virus posttranslational regulatory element (*WPRE*) that serves to enhance AAV-mediated transduction in mouse retina,³⁵ was packaged into SS.AAV2/9. This EGFP vector was spiked in with the SC.AAV2/9 vector (Figure 1B) and SS.AAV2/9 vector (Figure 1C) at 1×10^8 genomic copies per microliter (gc/ μ L) just before delivery to the mice so that the injected region of the retina could be identified by *in vivo* and *ex vivo* imaging. Another construct was made in which *NMNAT1* was driven by the ubiquitously expressing CAG promoter and followed by a T2A cleavage sequence, *EGFP*, and then *WPRE*. After translation in the cell, the *NMNAT1*-EGFP fusion protein was enzymatically separated at the T2A cleavage site³⁶ to avoid disruption of nominal protein conformations and kinetics. The construct was packaged into AAV2/Anc80, a

synthetic AAV vector that was generated by ancestral sequence reconstruction and that can transduce retinal cells efficiently both in mice and in non-human primates (Figure 1D).^{37,38} Finally, the same CASI.*NMNAT1* construct as described above was packaged into the AAV2/7m8 vector, which has been reported to transduce all retinal layers in mice following intravitreal injection (Figure 1E).³⁹ The SC.AAV2/9, SS.AAV2/9, and AAV2/Anc80 vectors were delivered by subretinal injection, whereas the AAV2/7m8 vector was delivered by intravitreal injection.

Gene Augmentation Using the Self-Complementary Vector Preserves Retinal Structure

Gene augmentation therapy using the SC.AAV2/9 vector stably preserved retinal structure in a dose-dependent manner when administered to 2-week-old *Nmnat1*^{V9M/V9M} mice. This finding was determined by measuring photoreceptor layer thickness in images collected *in vivo* using optical coherence tomography (OCT). Measurements from injected eyes were taken near the injection site in the inferior retina where rescue was anticipated to be most robust and in the superior retina that was far from the injection site. Measurements in the non-injected fellow eyes of both treated *Nmnat1*^{V9M/V9M} mice and treated age-matched wild-type control mice were acquired in the inferior retina in the plane equivalent to where the measurements were collected in the injected eyes (Figure 2).

Intermediate and high titer injections of the SC.AAV2/9 vector, 1×10^8 and 2×10^9 gc/ μ L, respectively, each provided significant rescue across the injected retina (Figure 3A). For example, in 9-month-old mutant mice, the average thicknesses of the inferior and superior photoreceptor layers of retinas injected with the 2×10^9 gc/ μ L dose were 100.0 ± 4.8 and 96.1 ± 6.4 μ m, respectively, whereas measurements in the inferior region of the fellow non-injected eyes averaged 31.3 ± 0.8 μ m (68.7 μ m difference from injected inferior retina, $p < 0.0001$, and 64.8 μ m difference from superior injected retina, $p < 0.0001$). Photoreceptor layer thickness in treated retinas of mutant mice were typically within $\sim 20\%$ of those collected from non-injected inferior retinas of wild-type mice. Within the treated mutant retinas, values tended to be similar ($p > 0.05$) at the inferior (near the injection site) and superior (far from the injection site) locations. However, photoreceptor layer thickness decreased by $\sim 20\%$ with distance from the injection site following the 1×10^8 gc/ μ L dose. Structural rescue following treatment with the lowest titer tested for this vector, 1×10^7 gc/ μ L, was more modest.

Because the impairment of *NMNAT1* activity may differ by mutation, understanding whether overexpression of this enzyme following gene augmentation, the viral particles, or the viral titer can cause toxicity is important. For this purpose, wild-type mice were injected with the SC.AAV2/9 vector using the three abovementioned titers. Across data collection time points for all doses, photoreceptor layer thickness was typically unaffected, with small but statistically significant differences being noted in only three instances (Figure 3B). The largest disparity was in the superior region of the injected retinas in which the thickness was decreased by 17.9 ± 6.9 μ m ($p = 0.039$) 9 months

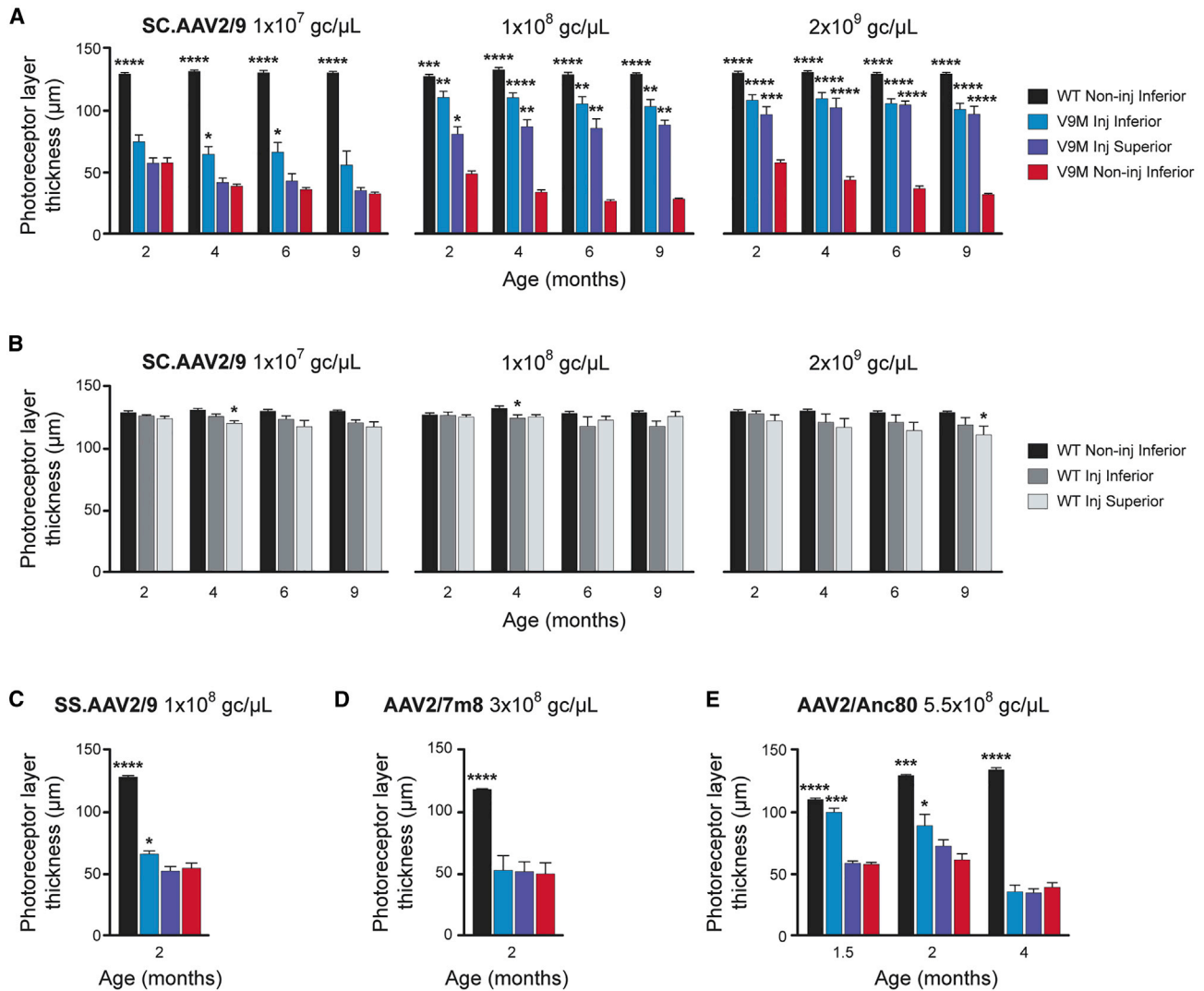


Figure 3. In Vivo Imaging Shows the SC.AAV2/9 Vector Provides Stable Rescue of Retinal Structure

(A) Photoreceptor layer thickness measurements from OCT images from 2- to 9-month-old mice after injection with the SC.AAV2/9 vector at 1×10^7 gc/ μ L (2, 4, 6, and 9 months; n = 8, 8, 5, 5 wild-type; n = 8, 7, 5, 4 mutant), 1×10^8 gc/ μ L (n = 8, 8, 4, 4 wild-type; n = 3, 4, 4, 4 mutant), and 2×10^9 gc/ μ L (n = 16, 16, 16, 15 wild-type; n = 10, 10, 9, 9 mutant). Comparisons of the inferior region of non-injected *Nmnat1*^{V9M/V9M} retinas with the inferior and superior regions of the fellow injected retinas and with the inferior region of non-injected wild-type littermate control retinas show that structural rescue is dose-dependent. (B) Measurements of the inferior region of non-injected wild-type retinas compared with the superior and inferior regions of the injected fellow retinas indicate little or no toxicity of the vector (see A for sample sizes). (C) The SS.AAV2/9 vector delivered at 1×10^8 gc/ μ L shows a modest rescue of the photoreceptor layer at 2 months of age (2 months: n = 10 wild-type; n = 9 mutant). (D) Photoreceptor layer thickness measurements show no detectable rescue by the AAV2/7m8 vector at 3×10^8 gc/ μ L at 2 months of age (2 months: n = 3 wild-type; n = 3 mutant). (E) A transient rescue of photoreceptor layer thickness, which did not persist to 4 months of age, was observed following the use of the AAV2/Anc80 vector at 5.5×10^8 gc/ μ L (1.5, 2, and 4 months: n = 4, 9, 13 wild-type; n = 4, 8, 15 mutant). Error bars represent the SEM. *p < 0.05, **p < 0.01, ***p < 0.001, ****p < 0.0001.

after the 2×10^9 gc/ μ L injection. However, given that the inferior region (near the injection site) of the same retina was unaffected, this decrease was unlikely to be due to toxicity.

Single-Stranded Vectors Do Not Stably Preserve Retinal Structure

In contrast to the SC.AAV2/9 vector, the SS.AAV2/9, AAV2/7m8, and AAV2/Anc80 vectors did not provide stable structural rescue

of the *Nmnat1*^{V9M/V9M} retina. At 2 months of age, the inferior region of mutant retinas injected with the SS.AAV2/9 vector showed a modest rescue of photoreceptor thickness (11.4 ± 4.3 μ m, p = 0.033) versus the same region of the non-injected fellow eye (Figure 3C), whereas the AAV2/7m8 vector had no effect (Figure 3D). The 5.5×10^8 gc/ μ L dose of the AAV2/Anc80 vector produced transient rescue in the mutant retina that did not persist beyond 2 months of age and was confined to the inferior region. At the 1.5- and

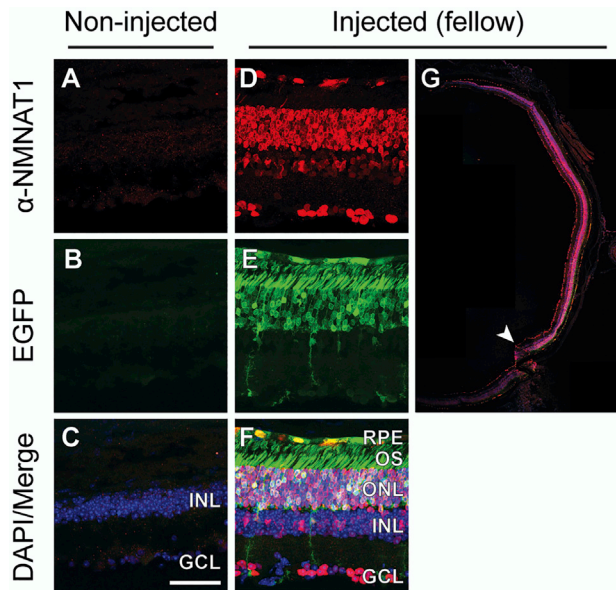


Figure 4. Ex vivo Imaging Shows Structural Rescue at Cellular Level in Retina Treated with the SC.AAV2/9 Vector

Immunolabeled retina from a representative 9-month-old *Nmnat1*^{V9M/V9M} mouse. (A–C) The non-injected retina has neither α -NMNAT1 antibody reactivity (red) nor EGFP expression (green). (D–F) Both signals are detected in the injected fellow retina. (G) A montage of the full retinal section, labeled with the α -NMNAT1 antibody, shows the extent of transgene expression across the retina. DAPI (blue) is the counterstain in (C), (F), and (G), and the white arrowhead indicates the injection site in (G). Images shown are from a 9-month-old *Nmnat1*^{V9M/V9M} mouse injected on P14 with SC.AAV2/9 at a titer of 2×10^9 gc/ μ L. Original magnification, $\times 63$; scale bar represents 50 μ m. RPE, retinal pigment epithelium; OS, outer segments; ONL, outer nuclear layer; INL, inner nuclear layer; GCL, ganglion cell layer.

2-month time points, respectively, the inferior region of AAV2/Anc80-treated retinas had photoreceptor thicknesses that were 42.0 ± 3.7 μ m ($p = 0.0005$) and 27.5 ± 9.9 μ m ($p = 0.045$) greater than that of the untreated fellow retinas (Figure 3E). No rescue was observed when the dose of the AAV2/Anc80 vector was decreased to 1×10^8 gc/ μ L (data not shown), and increasing the dose to $\geq 1 \times 10^9$ gc/ μ L failed due to apparent toxicity. The high titer injections of the AAV2/Anc80 vector caused detachment in some wild-type and some *Nmnat1*^{V9M/V9M} retinas by 6 weeks of age (Figure S1).^{40,41} To test whether the dilution buffer used with the AAV2/Anc80 vector contributed to this outcome, components of this solution were injected into wild-type mice under different conditions (i.e., modulating the concentrations of surfactant, salt, and fluorescein). These modifications to the reagent did not cause retinal damage as assessed by OCT or by histology (data not shown).

Nuclear Localization of Human NMNAT1 Is Observed across Cell Types in SC.AAV2/9-Treated Retinas

Ex vivo immunofluorescence imaging of retinas treated with the SC.AAV2/9 vector was performed using a custom chicken polyclonal α -human NMNAT1 antibody. This antibody displays no cross-reactivity with mouse NMNAT1 (Figure S2). Treated retinas showed

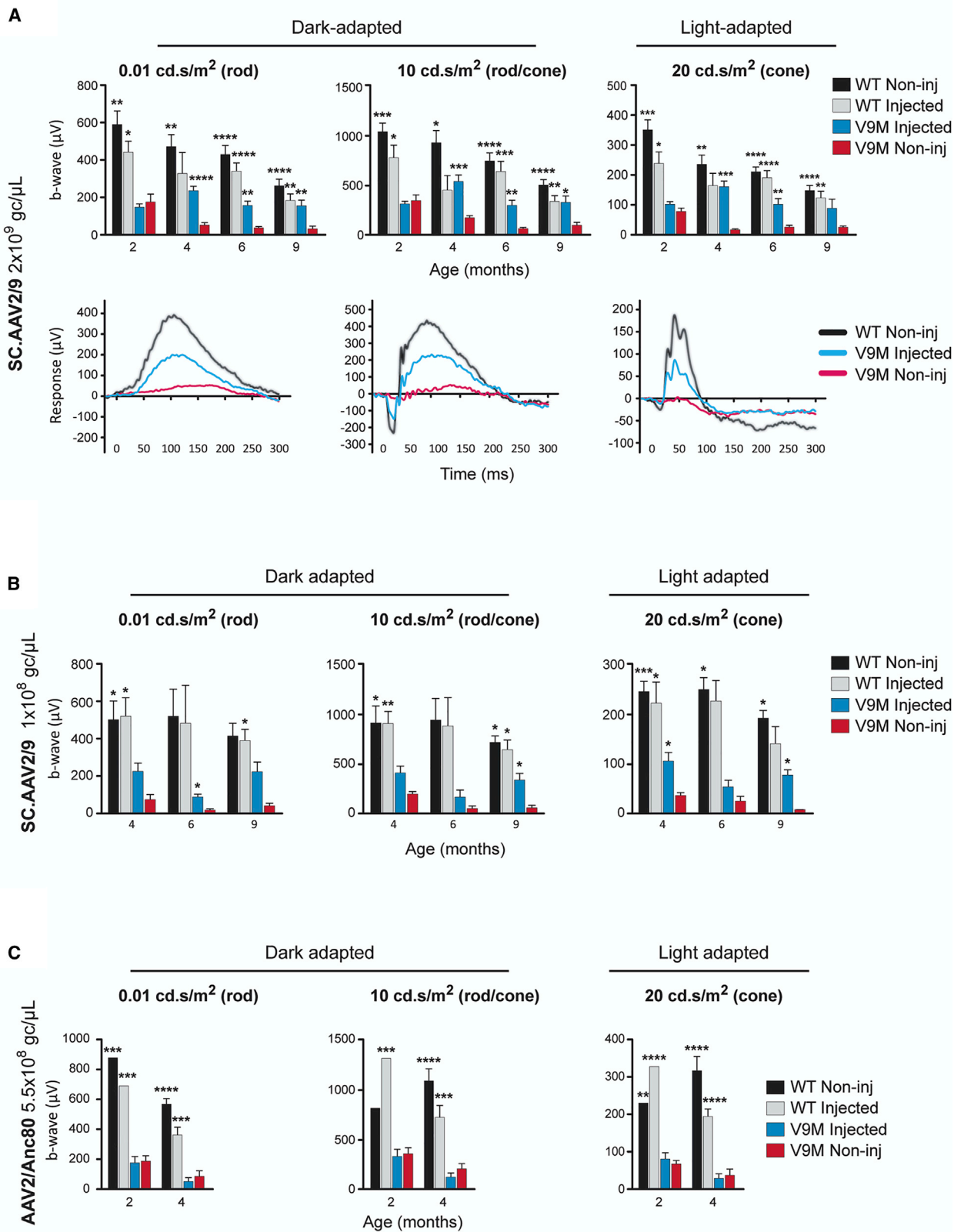
nuclear localization of human NMNAT1 in the retinal pigment epithelium (RPE), outer nuclear layer, inner nuclear layer, and ganglion cell layer, indicating transgene expression across cell types (Figures 4D–4F). Furthermore, an injection can transduce more than two-thirds of the tissue area (Figure 4G).

Gene Augmentation Using a Self-Complementary Vector Preserves Retinal Function

To assess whether structural rescue of the retina translated to preservation of function, we measured rod and cone photoreceptor function *in vivo* with ERG testing, a non-invasive procedure that records electrical responses of the retina to light stimulation. The intensity of the light was calibrated so that rod-mediated responses and mixed rod/cone-mediated responses were recorded separately when the mice were dark-adapted, and cone-mediated responses were recorded when the mice were light-adapted. For each stimulus condition, the magnitude of the ERG b-wave, which is mediated by ON bipolar cells,^{42,43} was used as an indirect indicator of the photoreceptor response⁴⁴ and a measure of inner retinal function. To directly assess photoreceptor function, the ERG a-wave^{45–47} was analyzed for the mixed rod/cone response; this near maximum stimulus condition was selected on the basis that, in normal mice, the a-wave is more robust in mixed rod/cone ERGs than in dimmer stimulus-elicited dark-adapted ERGs or in light-adapted ERGs.^{14,48–50}

Retinal function was preserved in eyes of mutant mice treated with the SC.AAV2/9 vector. With injection of the 2×10^9 gc/ μ L dose, the b-wave was significantly greater than that of the untreated fellow eye by 4 months of age for each stimulus condition and remained so through 6 months of age for the light-adapted condition. The b-wave remained significantly greater to at least 9 months of age for both dark-adapted conditions, and cone-isolated ERGs recorded at 9 months of age tended to be greater in the treated mutant eye than in the untreated fellow eye (Figure 5A, top row). For example, in 6-month-old mutant mice, the b-wave of the treated retina exceeded that of the fellow untreated retina for each condition: 156.1 ± 23.4 versus 36.0 ± 7.1 μ V ($p = 0.0013$) for the rod response, 293.6 ± 51.1 versus 62.0 ± 11.8 μ V ($p = 0.0034$) for the mixed rod/cone response, and 101.3 ± 18.6 versus 25.3 ± 6.2 μ V ($p = 0.0067$) for the cone response. Likewise, the a-wave was significantly greater for the treated eyes of the mutant mice than for the fellow untreated eyes by 4 months of age, and this effect remained through 9 months of age (Figure S3).

The responses associated with rescue in the *Nmnat1*^{V9M/V9M} retinas were consistently lower than those of the untreated wild-type retinas, and vector titer may have contributed to this effect. ERGs recorded from injected eyes of 9-month-old wild-type mice tended to be negatively correlated with dosage; the average response amplitude across the three stimulation conditions was 86% of normal with use of the 1×10^8 gc/ μ L titer versus 73% of normal with the 2×10^9 gc/ μ L titer. Regardless, the structure and implicit times of the rescued ERG waveforms were normal at all ages (Figure 5A, bottom row). The gradual



(legend on next page)

decline in ERG amplitudes observed in wild-type animals between 2 and 9 months of age is normal.^{44,51}

The SC.AAV2/9 vector at a lower dose of 1×10^8 gc/ μ L still showed evidence of functional rescue in the injected mutant retina (Figure 5B), whereas no sign of functional rescue by the AAV2/Anc80 vector at a similar dose of 5.5×10^8 gc/ μ L was observed at 2 months of age (Figure 5C), despite evidence of preserved retinal structure.

Self-Complementary Vector Activates *NMNAT1* Expression Earlier Than Single-Stranded Vectors

To understand why retinal structure and function were best preserved when treatment was delivered via the SC.AAV2/9 vector, we compared the early *NMNAT1* expression profiles of SC.AAV2/9, SS.AAV2/9, and AAV2/Anc80 delivery vectors in treated eyes of mixed C57BL/6J-129S6 wild-type mice. Injections occurred at around postnatal day 16 (P16), and each vector was used with a titer of 1×10^8 gc/ μ L. At 14 days post-injection, timed precisely for each animal, immunolabeling of *NMNAT1* delivered by the SC.AAV2/9 vector was observed in all retinal layers with particularly high density in the outer nuclear layer (Figure 6A). Conversely, in SS.AAV2/9- and AAV2/Anc80-injected retinas, detection of *NMNAT1* was sparse with relatively few photoreceptors labeled, even though the SS.AAV2/9 vector carried identical cargo and the AAV2/Anc80 vector has been shown to transduce the mouse retina photoreceptors with wide coverage.³⁷ *NMNAT1* was undetectable at 7 days post-injection, regardless of which of the three delivery vectors was used (data not shown). The greater efficiency of rod photoreceptor transduction by AAV2/Anc80 that we have reported previously³⁷ may be due to those mice having been injected at substantially older ages (6–8 weeks old) than the mice described herein.

A Successful Intervention Requires Transduction of Photoreceptors

To determine whether an earlier intervention would produce better efficacy from the AAV2/Anc80 vector, injections were performed in neonatal mice at P0 through P2. While most cell types, including cone photoreceptors, showed strong *NMNAT1* expression in these animals, expression in rod photoreceptors was relatively weak (Figure 6B); cones were distinguished by the location of their nuclei in the outermost rows of the outer nuclear layer (ONL).⁵² Given that AAV2/Anc80 efficiently transduces rod photoreceptors following subretinal injection in adult mice (6–8 weeks old),³⁷ and since another research group reported poor transduction of rods by other AAV vectors following subretinal injection of neonatal mice,⁵³ we did not pur-

sue neonatal injections using the SS.AAV2/9 or SC.AAV2/9 vectors. Similar to AAV2/Anc80 injection of neonatal mice, intravitreal delivery of *NMNAT1* via AAV2/7m8 in 2-week-old mice did not preserve the photoreceptor layer, as observed by OCT 4 weeks after injection, and we determined by immunohistochemistry that *NMNAT1* expression was absent in the outer retina, despite a strong inner retina signal (Figure 6C).

DISCUSSION

This study is the first demonstration of a gene therapy that successfully treats *NMNAT1*-associated retinal degeneration. Retinas of *Nmnat1*^{V9M/V9M} mice supplemented with a normal copy of human *NMNAT1* via AAV-mediated gene augmentation show preservation of both structure and function. This result was achieved using a self-complementary AAV vector that was more effective than single-stranded vectors delivering the same transgene. Data indicate that the rapid activation of gene expression associated with the self-complementary vector provided a better outcome by permitting widespread transduction of retinal cells within the narrow therapeutic window for this disease. Efficient transduction of photoreceptor cells appears to be necessary for therapeutic efficacy, and rescue of retinal structure tended to be more robust than that of function. The results presented suggest that, with further optimization, AAV-mediated gene augmentation therapy has the potential to benefit patients affected by *NMNAT1*-associated retinal degeneration.

Retinas of *Nmnat1*^{V9M/V9M} mice supplemented with a normal copy of human *NMNAT1* via AAV-mediated gene augmentation show preservation of structure and function for at least 9 months. This effect, which was dose-dependent, was achieved using the SC.AAV2/9 delivery vector. Although the highest viral titer used conferred the greatest effect, the observation that an intermediate titer also provided rescue suggests that high doses of AAV-*NMNAT1* may not be needed for a clinically effective therapy. In contrast to the SC.AAV2/9 vector, the three single-stranded AAV vectors did not provide sustained therapeutic effects. The SS.AAV2/9 vector, the direct counterpart of the SC.AAV2/9 vector, afforded only modest preservation of retinal structure in mice at 2 months of age. Similarly, the AAV2/Anc80 vector provided a transient structural benefit with no functional rescue. The AAV2/7m8 vector, delivered by intravitreal injection, did not transduce the outer retina and failed to provide a structural or functional benefit. In comparison to these single-stranded vectors, the self-complementary vector had a transgene expression profile that was comparatively faster, greater, and included more target cells, notably photoreceptors.

Figure 5. ERG Shows Preservation of Retinal Function after Treatment with SC.AAV2/9 Vector

(A) Retinas from *Nmnat1*^{V9M/V9M} mice treated with a 2×10^9 gc/ μ L dose of SC.AAV2/9 generated significantly larger rod, mixed rod/cone, and cone-isolating ERGs than did the untreated fellow retinas, as measured by the ERG b-wave. Measurements from the non-injected *Nmnat1*^{V9M/V9M} retinas are compared to injected fellow retinas and to non-injected and injected retinas of wild-type mice (age 2, 4, 6, 9 months: n = 6, 4, 14, 13 wild-type; 5, 9, 10, 9 mutant; top row). ERG waveforms from a 6-month-old treated *Nmnat1*^{V9M/V9M} mouse (treated retina, blue trace; untreated retina, red trace) and an age-matched wild-type littermate (untreated retina, black trace; bottom row). (B) ERG measurements to 9 months of age for mice injected with SC.AAV2/9 vector at the 1×10^8 gc/ μ L dose (age 4, 6, 9 months: n = 5, 3, 3 wild-type; n = 5, 4, 4 mutant). (C) ERG measurements to 4 months of age with the AAV2/Anc80 vector at the 5.5×10^8 gc/ μ L dose (age 2, 4 months: n = 1, 5 wild-type; n = 9, 5 mutant). Error bars represent the SEM. *p < 0.05, **p < 0.1, ***p < 0.001, ****p < 0.0001.

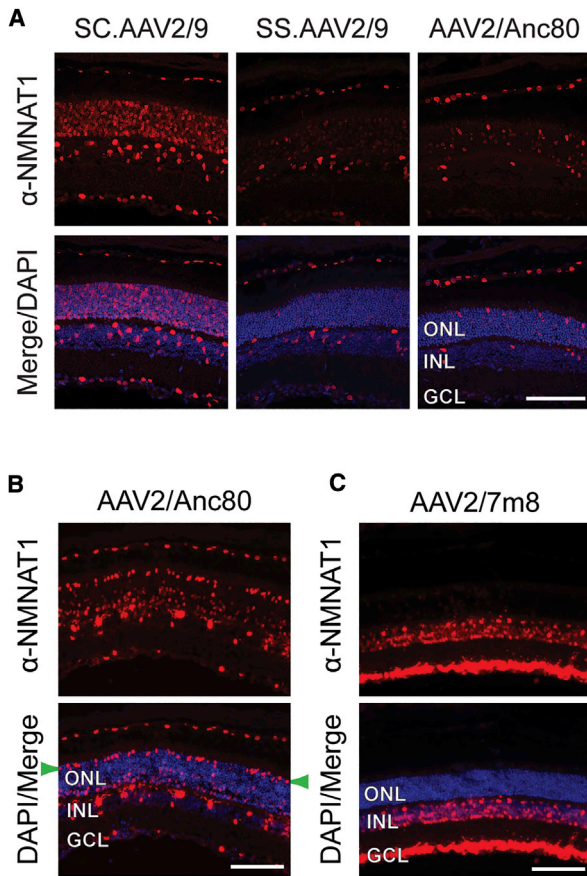


Figure 6. Vector-Specific Transgene Expression Profiles Indicate That Treatment of Photoreceptors Is Required for a Successful Therapy

(A) SC.AAV2/9, SS.AAV2/9, and AAV2/Anc80 vectors were delivered at 1×10^8 gc/ μ L to wild-type mice at age \sim P16. At precisely 14 days post-injection, dense α -NMNAT1 immunoreactivity (red) is visible in the retina (notably in the ONL) injected with the SC.AAV2/9 vector (left column), whereas this signal is sparse in age-matched retinas injected with either the SS.AAV2/9 (center column) or the AAV2/Anc80 (right column) vector. Original magnification, $\times 40$; scale bar represents 75 μ m. (B) A retina from a 5.5-week-old wild-type mouse that was injected with 3.5×10^9 gc/ μ L of AAV2/Anc80 at P1 shows strong α -NMNAT1 immunoreactivity (red) in virtually all cell types except for rod photoreceptors at 5 weeks post-injection. The labeled cells populating the outermost row of the ONL (flanked by green arrowheads) are cones. Original magnification, $\times 20$; scale bar represents 100 μ m. (C) Intravitreal injection of the AAV2/7m8 vector at 3×10^8 gc/ μ L in a 2-week-old control mouse generates strong NMNAT1 expression (red) in the INL and GCL but not in the ONL at 4 weeks post-treatment. DAPI (blue) is the counterstain in the bottom row of each panel. Original magnification, $\times 20$; scale bar represents 100 μ m. ONL, outer nuclear layer; INL, inner nuclear layer; GCL, ganglion cell layer.

The rapid activation of gene expression associated with the self-complementary vector permitted efficient transduction of rod photoreceptors within the narrow therapeutic window for this disease, leading to a substantially better outcome than for single-stranded vectors.¹⁴ The transgene is expressed quickly due to the double-stranded configuration of the self-complementary genome, which allows the rate-limiting step of second-strand synthesis to be circum-

vented.^{18,34,54–56} The *Nmnat1*^{V9M/V9M} mouse model has a narrow therapeutic window, bounded on the early side by immature rods that are unable to be transduced efficiently by AAV⁵³ and on the late side by the onset of the rapidly progressing disease. We hypothesize that the shorter latency for gene expression after transduction by the SC.AAV2/9 vector allowed for a more efficient treatment within these constraints.

Treatment with the self-complementary vector resulted in successful transduction of photoreceptors, which led to substantially better preservation of retinal structure and function. Two-week-old (i.e., \sim P16) mice were injected because AAV has been reported to transduce approximately twice as many rods when it is delivered at P21 versus P10 and has also been observed to have poor transduction of rods when delivered at neonatal ages.^{53,57,58} The injections were not delayed further because, despite the rapid transgene activation, more than a week was required to detect NMNAT1 expression in retinas of wild-type mice dosed with the SC.AAV2/9 delivery vector. SC.AAV has been observed in previous studies to produce low-level transgene expression in retinal cells that is detectable by immunofluorescence microscopy by 7 days post-injection.^{59–61} In the present study, it was not determined whether the relatively young age of the mice at the time of injection, the viral vector, or the DNA construct may have contributed to the latency in transgene expression. Because the co-injected *EGFP* was delivered via the more slowly activating SS.AAV, this marker was not informative for evaluating whether the *NMNAT1* transgene was rate-limiting. Furthermore, we found that early intervention with SS.AAVs was unsuccessful, likely because they did not transduce rods. Future experiments using cell type-specific promoters could help identify whether *NMNAT1* supplementation in photoreceptors is sufficient for treatment efficacy, and, if not, which other cell types are required. Success of this vector may also be due to higher levels of gene expression, and this will be further examined in future studies, as well.

In eyes treated with the SC.AAV2/9 delivery vector, the level of preservation was consistently greater and more stable for retinal structure than for function. The photoreceptor layer was only \sim 15%–25% thinner in treated mutant retinas than in wild-type retinas; however, ERG b-wave and a-wave amplitudes tended to be \sim 50% lower in treated mutant retinas as compared to untreated wild-type retinas. Despite early preservation of retinal structure in treated eyes of the mutant mice, functional rescue did not become apparent by ERG until after the 2-month time point. While the mechanism underlying this latency will require further investigation, the transient lack of a-wave rescue indicates direct photoreceptor involvement. Furthermore, the photoreceptor layer of wild-type retinas injected with the SC.AAV2/9 vector at the 2×10^9 gc/ μ L dose was only slightly thinner (\sim 1%–8%) than the same region of retina in the fellow non-injected eyes, but retinal function was reduced by \sim 25%. It is possible that the reduced ERG signal could be due to mechanical trauma from the injection procedure,⁶² however, damage to a small region would likely not affect the full-field ERG to this extent. Furthermore, ERG responses were not decreased in wild-type mice treated with the

1×10^8 gc/ μ L titer of SC.AAV2/9, suggesting that the reduced retinal function observed following injection of the higher dose of SC.AAV2/9 could be due to some toxicity of the vector. High levels of NMNAT1 itself could be associated with reduced retinal function, although this seems unlikely based on results of previous studies showing that high levels of NMNAT1 and NAD⁺ are not detrimental to neural cells.^{63–67} If excessive NMNAT1 can be toxic to cells, then with high titer delivery of the AAV2/Anc80 vector, inclusion of *WPRE* in the DNA construct may have driven transgene expression to levels that cause an inflammatory response. Regardless, the potential for toxicity by NMNAT1 overexpression in the retina needs to be investigated further. Other possible sources of toxicity include elements of the viral vector or a contaminant in the vector preparations,^{35,37,58,68,69} although we found no specific evidence for these candidates. It is possible that the CASI promoter, similar to some other broadly active promoters, could contribute some toxicity to AAV vectors, but further work is needed to assess this possibility.⁵⁸

The therapeutic effects of *NMNAT1* gene therapy reported in the present study provide evidence that gene augmentation therapy could be used to treat patients suffering from *NMNAT1*-associated retinal degeneration. Self-complementary AAV vectors have been successfully used to treat other neurodegenerative disorders such as spinal motor atrophy.²⁸ As indicated, additional studies will be needed to optimize *NMNAT1* gene therapy for clinical translation. For example, the ability of this therapy to target both cone and rod photoreceptors is likely to be important for clinical translation because foveal atrophy is a common feature associated with *NMNAT1*-disease.^{1–4} For patients with intact foveas, maintaining healthy rods would support the long-term viability of the treated central and peripheral cones,^{70,71} and for patients with foveal atrophy, treatment outside of the macula to preserve sight via peripheral cones and rods could also provide considerable benefit. Because gene augmentation has the potential to preserve vision in *NMNAT1*-disease patients from childhood onward, the availability of such a therapy would improve quality-of-life for this global patient population, especially in regions where blindness is associated with poverty, denial of access to education, and increased mortality.^{72,73}

MATERIALS AND METHODS

Mouse Lines

The p.V9M-*Nmnat1* mouse line was derived previously from an *N*-ethyl-*N*-nitrosourea (ENU) mutagenesis screen.¹⁴ To increase fecundity, the original C57BL/6J line was alternately outcrossed with wild-type 129S6/SvEvTac mice (Taconic, Rensselaer, NY, USA) and wild-type C57BL/6J mice (The Jackson Laboratory, Bar Harbor, ME, USA) to maintain a mixed C57BL/6J-129S6 genetic background. Wild-type CD1-IGS mice (Charles River, Wilmington, MA, USA), used only to screen for vector component toxicity, were maintained separately. Male and female mice were used in experiments without preference.

Animal Husbandry

Mice were fed 4% fat rodent diet and water *ad libitum* and housed in a 12-h light/12-h dark cycle. This study conformed to the Association

for Research in Vision and Ophthalmology Statement for the Use of Animals in Ophthalmic and Vision Research, and all procedures were approved by the Animal Care and Use Committee.

Genotyping

A tissue biopsy was prepared for polymerase chain reaction (PCR) using All^{le}-In-One mouse tail direct lysis buffer (Allele Biotech, San Diego, CA, USA) according to the manufacturer's instructions. PCR was performed using the forward primer 5'-CATG GCTGTGCTGAGGTG-3' (intron 1) and reverse primer 5'-AACA GCCTGAGGTGCATGTT-3' (exon 2) to amplify a 691-bp region of *Nmnat1* that includes codon 9. The 20- μ L PCR reactions had final concentrations of 200 μ mol/L for each primer, 200 nmol/L for each of the deoxyribonucleotide triphosphates (dNTPs) (deoxyadenosine triphosphate [dATP], deoxyguanosine triphosphate [dGTP], deoxythymidine triphosphate [dTTP], and deoxycytidine triphosphate [dCTP]), 2 mmol/L MgCl₂, and 1 U of Hot FirePol DNA polymerase (Solis BioDyne, Tartu, Estonia). The thermocycling protocol was 95°C for 14 minutes; 30 cycles of 95°C for 45 s, 53°C for 45 s, 72°C for 30 s; and 72°C for 7 min. Next, the amplified product was subjected to Sanger sequencing using primer 5'-ACGTATTGCCC CACCTGTCT-3', and the resulting data were then analyzed at c.25 to identify each mouse as being wild-type, *Nmnat1*^{WT/V9M}, or *Nmnat1*^{V9M/V9M}.

DNA Construct and AAV Vector Preparation

A codon-optimized human *NMNAT1* cDNA (Figure 1A), designed by DNA 2.0 (Menlo Park, CA, USA) and synthesized into a gBlock gene fragment (Integrated DNA Technologies, Coralville, IA, USA), was incorporated into constructs that were then packaged into recombinant AAV viral vectors. Plasmids containing the complete constructs were generated using standard endotoxin-free molecular cloning techniques and validated by sequencing *NMNAT1* and regions crossing ligation sites. AAV was prepared by the Grousebeck Gene Therapy Center of Massachusetts Eye and Ear, as described previously.³⁷ Purified virus was collected and titered in a final buffer containing 1 \times phosphate-buffered saline (PBS), 35 mM NaCl, and 0.001% Pluronic F68 surfactant. The same buffer was used to further dilute the virus, if required, to achieve the target dose. To assist with the injection procedure, <0.25% of fluorescein (AK-Fluor, Akorn, Lake Forest, IL, USA) was mixed into the working solution as a tracer.

Anesthesia

For general anesthesia, a mixture of ketamine/xylazine was delivered by intraperitoneal injection. Two-week-old mice received a dose of 37.5 mg/kg ketamine and 3.8 mg/kg xylazine and adult mice received a dose of 100 mg/kg ketamine and 20 mg/kg xylazine. To counteract the formation of anesthesia-induced corneal opacities, a 2 mg/kg dose of yohimbine HCl (Wedgewood Pharmacy, Swedesboro, NJ, USA) was administered by subcutaneous injection immediately after each recovery procedure in which ketamine/xylazine was used.^{74,75} For neonatal mice, general anesthesia by hypothermia was induced by indirect exposure to ice.⁷⁶

Virus Delivery

In 2-week-old mice, a Micro4 microinjection pump with an RPE kit (World Precision Instruments, Sarasota, FL, USA) was used to deliver the viral vectors into either the subretinal space or the vitreous chamber. Pupils were dilated using either tropicamide (1%) or a mixture of tropicamide (0.25%), phenylephrine HCl (1.25%), and cyclopentolate (0.5%). Mice were anesthetized with ketamine/xylazine, and local anesthesia was administered topically using proparacaine HCl (0.5%). Next, the eye was propped and a 30G syringe needle was used to puncture the superior-temporal sclera and retina immediately posterior to the limbus to make an entry route for a blunt-end 33G cannula.

For subretinal injections, the cannula tip was positioned in the subretinal space of the inferior-nasal quadrant of the eye, 0.75 μL of vector was injected, and the formation of a bleb was confirmed by visualization. The cannula was held in place for approximately 3 s following injection to avoid reflux of the vector and then gently removed from the eye. Finally, the entry wound was treated by tamponade with a cotton swab. The eyes were then hydrated with artificial tears (Blink Tears, Abbott Laboratories, Chicago, IL, USA), and the mice recovered from anesthesia on a heating pad. The procedure for intravitreal injection of two-week-old mice was identical, except that the cannula tip was positioned in the center of the vitreous chamber during injection.

The FemtoJet 4i microinjection system (Eppendorf, Hamburg, Germany) was used to deliver subretinal injections to neonates. While the mice were anesthetized on ice, the tip of a 30G hypodermic needle was used to separate the upper and lower eyelids. The eye was propped and a custom beveled glass needle (catalog no. C060609, Origio, Trumbull, CT, USA) was directly inserted through the sclera and positioned in the underlying subretinal space. A single bolus of 0.5 μL of vector was administered, after which the needle was held in place for approximately 3 s to avoid reflux and then gently removed. The mice recovered from anesthesia on a heating pad.

In Vivo Retinal Imaging

En face and cross-sectional images of the retina were acquired using fundus photography and spectral domain OCT, respectively, and as described previously¹⁴ with the following modifications: some fundus images were taken through a filter that allows for visualization of EGFP and therefore early evaluation of AAV injection quality, the rectangular volume OCT scans were taken at multiple locations across the retina so that inferior and superior regions could be measured accurately, and 10 B-scans were registered/averaged to generate final OCT images. Using InVivoVue OCT software (BiopTigen), four equally spaced electronic caliper measurements were made from the outer plexiform layer to the RPE to measure photoreceptor layer thickness. Across the time points tested (2, 4, 6, and 9 months, unless otherwise stated) for each reagent, the sample sizes were as follows: SC.AAV2/9 1×10^7 gc/ μL (n = 8, 8, 5, 5 wild-type; n = 8, 7, 5, 4 mutant), SC.AAV2/9 1×10^8 gc/ μL (n = 8, 8, 4, 4 wild-type; n = 3, 4, 4, 4 mutant), SC.AAV2/9 2×10^9 gc/ μL (n = 16, 16, 16, 15

wild-type; n = 10, 10, 9, 9 mutant), SS.AAV2/9 1×10^8 gc/ μL (age 2 months: n = 10 wild-type; n = 9 mutant), AAV2/7m8 3×10^8 gc/ μL (age 2 months: n = 3 wild-type; n = 3 mutant), AAV2/Anc80 5.5×10^8 gc/ μL (age 1.5, 2, and 4 months, n = 4, 9, 13; wild-type, n = 4, 8, 15 mutant).

Electroretinography

Full-field, flash ERGs were collected from the mice as described previously.¹⁴ Briefly, mice were dark adapted overnight, and rod responses and mixed rod/cone responses were generated using a 0.01 $\text{cd} \cdot \text{s}/\text{m}^2$ (scotopic) and 10 $\text{cd} \cdot \text{s}/\text{m}^2$ (scotopic) broadband light stimulus, respectively. Next, the mice were light adapted by exposure to a steady 30 cd/m^2 (photopic) broadband light for 10 min; this rod-suppressing light remained on in the background during the acquisition of cone-isolated responses to a 20 $\text{cd} \cdot \text{s}/\text{m}^2$ (photopic) broadband light stimulus. Across the time points and stimulus conditions tested for each reagent, the sample sizes were as follows: SC.AAV2/9 1×10^8 gc/ μL (age 4, 6, 9 months: n = 5, 3, 3 wild-type; n = 5, 4, 4 mutant), SC.AAV2/9 2×10^9 gc/ μL (age 2, 4, 6, 9 months: n = 6, 4, 14, 13 wild-type; 5, 9, 10, 9 mutant), AAV2/Anc80 5.5×10^8 gc/ μL (age 2, 4 months: n = 1, 5 wild-type; n = 9, 5 mutant).

Statistical Analysis

Statistical analyses were completed in Prism version 8.2.1 (GraphPad, San Diego, CA, USA). For OCT and ERG time courses, a two-way ANOVA was performed using a mixed-effects regression model. When analyzing the effect of a treatment, the inferior retina of the non-injected eye was used as the negative control to which the means of all other measurements were compared. The Dunnett *post hoc* test was used to account for type I error generated from multiple comparisons testing. Analyses of the effects of injection and all quantitative data are reported as the mean \pm SEM.

Anti-Human NMNAT1 Antibody Development

Purified, full-length human NMNAT1 protein was used by Aves Labs (Tigard, OR, USA) as the antigen to generate polyclonal antibodies in chicken. The resulting antibody reacts strongly against human NMNAT1 without cross-reacting with the murine ortholog (Figure S2).

Immunohistochemistry and Ex Vivo Retinal Imaging

Mice were euthanized by CO_2 asphyxiation and immediately perfused through the heart using a Masterflex peristaltic pump (Cole-Parmer, Vernon Hills, IL, USA). Each animal was perfused first with 0.13 mol/L PBS (pH 7.2–7.4) that contained 2 U of heparin/mL until the perfusate became clear, and this was followed by perfusion of ~ 40 mL of 2% paraformaldehyde (PFA). Both solutions were warmed to $\sim 37^\circ\text{C}$ at the time of perfusion. A small vessel cauterizer (catalog no. 18000-00, Fine Science Tools, Foster City, CA, USA) was used to mark the cornea immediately anterior to the superior limbus. Eyes were enucleated, incubated at 2% PFA for 30 min at room temperature, the anterior segment was removed, and then the remaining eye cup was incubated once again in 2% PFA for 30 min at room temperature before being immersed in 30% sucrose at room temperature for

at least 1 h. Eye cups were embedded, sectioned at 10- μ L thickness by cryotomy, immunolabeled and stained, and imaged using either the Eclipse Ti fluorescence microscope (Nikon, Tokyo, Japan) or the TCS SP8 confocal microscope (Leica, Wetzlar, Germany), as described previously.¹⁴ The number of mice evaluated in Figure 6 were n = 2 per condition for (A), n > 4 for (B), and n = 3 for (C).

SUPPLEMENTAL INFORMATION

Supplemental Information can be found online at <https://doi.org/10.1016/j.omtm.2020.07.003>.

AUTHOR CONTRIBUTIONS

Conceptualization, E.A.P., L.H.V., and S.H.G.; Methodology, E.A.P., L.H.V., S.H.G., and R.X.; Formal Analysis, S.H.G., R.F., E.H., and M.J.S.; Investigation, S.H.G., R.F., E.H., M.J.S., E.E.B., and B.S.P.; Writing, S.H.G., E.A.P., and E.E.B.

CONFLICTS OF INTEREST

L.H.V. holds founder equity in GenSight Biologics, is a consultant to a number of biotech and pharmaceutical companies, and is an inventor on gene therapy patents, including Anc80, which are licensed to various entities. The remaining authors declare no competing interests.

ACKNOWLEDGMENTS

This research was supported by funding from NEI grant EY012910 (to E.A.P.), the Foundation Fighting Blindness and the Gavin R. Stevens Foundation (to E.A.P. and L.H.V.), the Sara Elizabeth O'Brien Trust (to S.H.G.), Fight for Sight (to S.H.G.), and NIH grant P30 EY014104 (to the MEEI Ophthalmology Core). Furthermore, the authors are grateful to Dr. Mathias Ziegler (University of Bergen) for providing purified human NMNAT1 that was used as the antigen for the antibody generation, and Dr. Rosario Fernandez-Godino (Massachusetts Eye & Ear) for providing cultured ARPE-19 cells.

REFERENCES

- Chiang, P.W., Wang, J., Chen, Y., Fu, Q., Zhong, J., Chen, Y., Yi, X., Wu, R., Gan, H., Shi, Y., et al. (2012). Exome sequencing identifies *NMNAT1* mutations as a cause of Leber congenital amaurosis. *Nat. Genet.* *44*, 972–974.
- Koenekoop, R.K., Wang, H., Majewski, J., Wang, X., Lopez, I., Ren, H., Chen, Y., Li, Y., Fishman, G.A., Genead, M., et al.; Finding of Rare Disease Genes (FORGE) Canada Consortium (2012). Mutations in *NMNAT1* cause Leber congenital amaurosis and identify a new disease pathway for retinal degeneration. *Nat. Genet.* *44*, 1035–1039.
- Perrault, I., Hanein, S., Zanlonghi, X., Serre, V., Nicouleau, M., Defoort-Delhemmes, S., Delphin, N., Fares-Taie, L., Gerber, S., Xerri, O., et al. (2012). Mutations in *NMNAT1* cause Leber congenital amaurosis with early-onset severe macular and optic atrophy. *Nat. Genet.* *44*, 975–977.
- Falk, M.J., Zhang, Q., Nakamaru-Ogiso, E., Kannabiran, C., Fonseca-Kelly, Z., Chakarova, C., Audo, I., Mackay, D.S., Zeitz, C., Borman, A.D., et al. (2012). *NMNAT1* mutations cause Leber congenital amaurosis. *Nat. Genet.* *44*, 1040–1045.
- Nash, B.M., Symes, R., Goel, H., Dinger, M.E., Bennetts, B., Grigg, J.R., and Jamieson, R.V. (2018). *NMNAT1* variants cause cone and cone-rod dystrophy. *Eur. J. Hum. Genet.* *26*, 428–433.
- Garavaglia, S., D'Angelo, I., Emanuelli, M., Carnevali, F., Pierella, F., Magni, G., and Rizzi, M. (2002). Structure of human NMN adenylyltransferase. A key nuclear enzyme for NAD homeostasis. *J. Biol. Chem.* *277*, 8524–8530.
- Belenky, P., Bogan, K.L., and Brenner, C. (2007). NAD⁺ metabolism in health and disease. *Trends Biochem. Sci.* *32*, 12–19.
- Lau, C., Niere, M., and Ziegler, M. (2009). The NMN/NaMN adenylyltransferase (NMNAT) protein family. *Front. Biosci.* *14*, 410–431.
- Chiarugi, A., Dölle, C., Felici, R., and Ziegler, M. (2012). The NAD metabolome—a key determinant of cancer cell biology. *Nat. Rev. Cancer* *12*, 741–752.
- Sasaki, Y., Margolin, Z., Borgo, B., Havranek, J.J., and Milbrandt, J. (2015). Characterization of Leber's congenital amaurosis-associated *NMNAT1* mutants. *J. Biol. Chem.* *290*, 17228–17238.
- Coppieters, F., Todeschini, A.L., Fujimaki, T., Baert, A., De Bruyne, M., Van Cauwenbergh, C., Verdin, H., Bauwens, M., Ongenaert, M., Kondo, M., et al. (2015). Hidden genetic variation in LCA9-associated congenital blindness explained by 5'UTR mutations and copy-number variations of *NMNAT1*. *Hum. Mutat.* *36*, 1188–1196.
- Conforti, L., Janackova, L., Wagner, D., Mazzola, F., Cialabrini, L., Di Stefano, M., Orsomando, G., Magni, G., Bendotti, C., Smyth, N., and Coleman, M. (2011). Reducing expression of NAD⁺ synthesizing enzyme *NMNAT1* does not affect the rate of Wallerian degeneration. *FEBS J.* *278*, 2666–2679.
- Berger, F., Lau, C., Dahlmann, M., and Ziegler, M. (2005). Subcellular compartmentation and differential catalytic properties of the three human nicotinamide mononucleotide adenylyltransferase isoforms. *J. Biol. Chem.* *280*, 36334–36341.
- Greenwald, S.H., Charette, J.R., Stanisewska, M., Shi, L.Y., Brown, S.D.M., Stone, L., Liu, Q., Hicks, W.L., Collin, G.B., Bowl, M.R., et al. (2016). Mouse models of *NMNAT1*-Leber congenital amaurosis (LCA9) recapitulate key features of the human disease. *Am. J. Pathol.* *186*, 1925–1938.
- Greenwald, S.H., and Pierce, E.A. (2019). Parthanatos as a cell death pathway underlying retinal disease. *Adv. Exp. Med. Biol.* *1185*, 323–327.
- Carvalho, L.S., and Vandenberghe, L.H. (2015). Promising and delivering gene therapies for vision loss. *Vision Res.* *111*, 124–133.
- Ong, T., Pennesi, M.E., Birch, D.G., Lam, B.L., and Tsang, S.H. (2019). Adeno-associated viral gene therapy for inherited retinal disease. *Pharm. Res.* *36*, 34.
- McCarty, D.M. (2008). Self-complementary AAV vectors; advances and applications. *Mol. Ther.* *16*, 1648–1656.
- Lloyd, A., Piglowska, N., Ciulla, T., Pitluck, S., Johnson, S., Buessing, M., and O'Connell, T. (2019). Estimation of impact of *RPE65*-mediated inherited retinal disease on quality of life and the potential benefits of gene therapy. *Br. J. Ophthalmol.* *103*, 1610–1614.
- Lam, B.L., Davis, J.L., Gregori, N.Z., MacLaren, R.E., Girach, A., Verriotto, J.D., Rodriguez, B., Rosa, P.R., Zhang, X., and Feuer, W.J. (2019). Choroideremia gene therapy phase 2 clinical trial: 24-month results. *Am. J. Ophthalmol.* *197*, 65–73.
- Ghazi, N.G., Abboud, E.B., Nowilaty, S.R., Alkuraya, H., Alhommadi, A., Cai, H., Hou, R., Deng, W.T., Boye, S.L., Almaghamsi, A., et al. (2016). Treatment of retinitis pigmentosa due to *MERTK* mutations by ocular subretinal injection of adeno-associated virus gene vector: results of a phase I trial. *Hum. Genet.* *135*, 327–343.
- ClinicalTrials.gov. Achromatopsia. <https://clinicaltrials.gov/ct2/results?cond=Achromatopsia&term=&cntry=&state=&city=&dist=>.
- ClinicalTrials.gov. X-linked retinoschisis. <https://clinicaltrials.gov/ct2/results?cond=X-linked+retinoschisis&term=&cntry=&state=&city=&dist=>.
- Dyka, F.M., Molday, L.L., Chiodo, V.A., Molday, R.S., and Hauswirth, W.W. (2019). Dual *ABCA4*-AAV vector treatment reduces pathogenic retinal A2E accumulation in a mouse model of autosomal recessive Stargardt disease. *Hum. Gene Ther.* *30*, 1361–1370.
- McCullough, K.T., Boye, S.L., Fajardo, D., Calabro, K., Peterson, J.J., Strang, C.E., Chakraborty, D., Gloskowski, S., Haskett, S., Samuelsson, S., et al. (2019). Somatic gene editing of *GUCY2D* by AAV-CRISPR/Cas9 alters retinal structure and function in mouse and macaque. *Hum. Gene Ther.* *30*, 571–589.
- Alves, C.H., and Wijnholds, J. (2018). AAV gene augmentation therapy for CRB1-associated retinitis pigmentosa. *Methods Mol. Biol.* *1715*, 135–151.
- Ofri, R., Averbukh, E., Ezra-Elia, R., Ross, M., Honig, H., Obolensky, A., Rosov, A., Hauswirth, W.W., Gootwine, and Banin, E. (2018). Six years and counting: restoration of photopic retinal function and visual behavior following gene augmentation therapy in a sheep model of CNGA3 achromatopsia. *Hum. Gene Ther.* *29*, 1376–1386.

28. Wirth, B., Karakaya, M., Kye, M.J., and Mendoza-Ferreira, N. (2020). Twenty-five years of spinal muscular atrophy research: from phenotype to genotype to therapy, and what comes next. *Annu. Rev. Genomics Hum. Genet.* Published online January 31, 2020. 10.1146/annurev-genom-102319-103602.
29. Burgess-Brown, N.A., Sharma, S., Sobott, F., Loenarz, C., Oppermann, U., and Gileadi, O. (2008). Codon optimization can improve expression of human genes in *Escherichia coli*: a multi-gene study. *Protein Expr. Purif.* 59, 94–102.
30. Gustafsson, C., Govindarajan, S., and Minshull, J. (2004). Codon bias and heterologous protein expression. *Trends Biotechnol.* 22, 346–353.
31. Ill, C.R., and Chiou, H.C. (2005). Gene therapy progress and prospects: recent progress in transgene and RNAi expression cassettes. *Gene Ther.* 12, 795–802.
32. Foster, H., Sharp, P.S., Athanasopoulos, T., Trollet, C., Graham, I.R., Foster, K., Wells, D.J., and Dickson, G. (2008). Codon and mRNA sequence optimization of microdystrophin transgenes improves expression and physiological outcome in dystrophic mdx mice following AAV2/8 gene transfer. *Mol. Ther.* 16, 1825–1832.
33. Sack, B.K., Merchant, S., Markusic, D.M., Nathwani, A.C., Davidoff, A.M., Byrne, B.J., and Herzog, R.W. (2012). Transient B cell depletion or improved transgene expression by codon optimization promote tolerance to factor VIII in gene therapy. *PLoS ONE* 7, e37671.
34. McCarty, D.M., Monahan, P.E., and Samulski, R.J. (2001). Self-complementary recombinant adeno-associated virus (scAAV) vectors promote efficient transduction independently of DNA synthesis. *Gene Ther.* 8, 1248–1254.
35. Patrício, M.I., Barnard, A.R., Orlans, H.O., McClements, M.E., and MacLaren, R.E. (2017). Inclusion of the woodchuck hepatitis virus posttranscriptional regulatory element enhances AAV2-driven transduction of mouse and human retina. *Mol. Ther. Nucleic Acids* 6, 198–208.
36. Kim, J.H., Lee, S.R., Li, L.H., Park, H.J., Park, J.H., Lee, K.Y., Kim, M.K., Shin, B.A., and Choi, S.Y. (2011). High cleavage efficiency of a 2A peptide derived from porcine teschovirus-1 in human cell lines, zebrafish and mice. *PLoS ONE* 6, e18556.
37. Zinn, E., Pacouret, S., Khaychuk, V., Turunen, H.T., Carvalho, L.S., Andres-Mateos, E., Shah, S., Shelke, R., Maurer, A.C., Plovie, E., et al. (2015). In silico reconstruction of the viral evolutionary lineage yields a potent gene therapy vector. *Cell Rep.* 12, 1056–1068.
38. Carvalho, L.S., Xiao, R., Wassmer, S.J., Langsdorf, A., Zinn, E., Pacouret, S., Shah, S., Comander, J.I., Kim, L.A., Lim, L., and Vandenberghe, L.H. (2018). Synthetic adeno-associated viral vector efficiently targets mouse and nonhuman primate retina in vivo. *Hum. Gene Ther.* 29, 771–784.
39. Dalkara, D., Byrne, L.C., Klimczak, R.R., Visel, M., Yin, L., Merigan, W.H., Flannery, J.G., and Schaffer, D.V. (2013). In vivo-directed evolution of a new adeno-associated virus for therapeutic outer retinal gene delivery from the vitreous. *Sci. Transl. Med.* 5, 189ra76.
40. Zarranz-Ventura, J., Keane, P.A., Sim, D.A., Llorens, V., Tufail, A., Satta, S.R., Dick, A.D., Lee, R.W., Pavesio, C., Denniston, A.K., and Adan, A.; EQUATOR Study Group (2016). Evaluation of objective vitritis grading method using optical coherence tomography: influence of phakic status and previous vitrectomy. *Am. J. Ophthalmol* 161, 172–180.e1-4.
41. Saito, M., Barbazzetto, I.A., and Spaide, R.F. (2013). Intravitreal cellular infiltrate imaged as punctate spots by spectral-domain optical coherence tomography in eyes with posterior segment inflammatory disease. *Retina* 33, 559–565.
42. Stockton, R.A., and Slaughter, M.M. (1989). B-wave of the electroretinogram. A reflection of ON bipolar cell activity. *J. Gen. Physiol.* 93, 101–122.
43. Bush, R.A., and Sieving, P.A. (1996). Inner retinal contributions to the primate photopic fast flicker electroretinogram. *J. Opt. Soc. Am. A Opt. Image Sci. Vis.* 13, 557–565.
44. Greenwald, S.H., Kuchenbecker, J.A., Roberson, D.K., Neitz, M., and Neitz, J. (2014). S-opsin knockout mice with the endogenous M-opsin gene replaced by an L-opsin variant. *Vis. Neurosci.* 31, 25–37.
45. Robson, J.G., Saszik, S.M., Ahmed, J., and Frishman, L.J. (2003). Rod and cone contributions to the a-wave of the electroretinogram of the macaque. *J. Physiol.* 547, 509–530.
46. Tanimoto, N., Muehlfriedel, R.L., Fischer, M.D., Fahl, E., Humphries, P., Biel, M., and Seeliger, M.W. (2009). Vision tests in the mouse: functional phenotyping with electroretinography. *Front. Biosci.* 14, 2730–2737.
47. Kinoshita, J., and Peachey, N.S. (2018). Noninvasive electroretinographic procedures for the study of the mouse retina. *Curr. Protoc. Mouse Biol.* 8, 1–16.
48. Saszik, S.M., Robson, J.G., and Frishman, L.J. (2002). The scotopic threshold response of the dark-adapted electroretinogram of the mouse. *J. Physiol.* 543, 899–916.
49. Peachey, N.S., Goto, Y., al-Ubaidi, M.R., and Naash, M.I. (1993). Properties of the mouse cone-mediated electroretinogram during light adaptation. *Neurosci. Lett.* 162, 9–11.
50. Ho, T., Vessey, K.A., Cappai, R., Dinet, V., Mascarelli, F., Ciccostoto, G.D., and Fletcher, E.L. (2012). Amyloid precursor protein is required for normal function of the rod and cone pathways in the mouse retina. *PLoS ONE* 7, e29892.
51. Gresh, J., Goletz, P.W., Crouch, R.K., and Rohrer, B. (2003). Structure-function analysis of rods and cones in juvenile, adult, and aged C57BL/6 and Balb/c mice. *Vis. Neurosci.* 20, 211–220.
52. Carter-Dawson, L.D., and LaVail, M.M. (1979). Rods and cones in the mouse retina. II. Autoradiographic analysis of cell generation using tritiated thymidine. *J. Comp. Neurol.* 188, 263–272.
53. Petit, L., Ma, S., Cheng, S.Y., Gao, G., and Punzo, C. (2017). Rod outer segment development influences AAV-mediated photoreceptor transduction after subretinal injection. *Hum. Gene Ther.* 28, 464–481.
54. Carter, B.J., Khoury, G., and Rose, J.A. (1972). Adenovirus-associated virus multiplication. IX. Extent of transcription of the viral genome in vivo. *J. Virol.* 10, 1118–1125.
55. Sipo, I., Fechner, H., Pinkert, S., Suckau, L., Wang, X., Weger, S., and Poller, W. (2007). Differential internalization and nuclear uncoating of self-complementary adeno-associated virus pseudotype vectors as determinants of cardiac cell transduction. *Gene Ther.* 14, 1319–1329.
56. Wang, J., Xie, J., Lu, H., Chen, L., Hauck, B., Samulski, R.J., and Xiao, W. (2007). Existence of transient functional double-stranded DNA intermediates during recombinant AAV transduction. *Proc. Natl. Acad. Sci. USA* 104, 13104–13109.
57. Xiong, W., MacColl Garfinkel, A.E., Li, Y., Benowitz, L.L., and Cepko, C.L. (2015). NRF2 promotes neuronal survival in neurodegeneration and acute nerve damage. *J. Clin. Invest.* 125, 1433–1445.
58. Xiong, W., Wu, D.M., Xue, Y., Wang, S.K., Chung, M.J., Ji, X., Rana, P., Zhao, S.R., Mai, S., and Cepko, C.L. (2019). AAV cis-regulatory sequences are correlated with ocular toxicity. *Proc. Natl. Acad. Sci. USA* 116, 5785–5794.
59. Natkunarajah, M., Trittbach, P., McIntosh, J., Duran, Y., Barker, S.E., Smith, A.J., Nathwani, A.C., and Ali, R.R. (2008). Assessment of ocular transduction using single-stranded and self-complementary recombinant adeno-associated virus serotype 2/8. *Gene Ther.* 15, 463–467.
60. Kong, F., Li, W., Li, X., Zheng, Q., Dai, X., Zhou, X., Boye, S.L., Hauswirth, W.W., Qu, J., and Pang, J.J. (2010). Self-complementary AAV5 vector facilitates quicker transgene expression in photoreceptor and retinal pigment epithelial cells of normal mouse. *Exp. Eye Res.* 90, 546–554.
61. Yokoi, K., Kachi, S., Zhang, H.S., Gregory, P.D., Spratt, S.K., Samulski, R.J., and Campochiaro, P.A. (2007). Ocular gene transfer with self-complementary AAV vectors. *Invest. Ophthalmol. Vis. Sci.* 48, 3324–3328.
62. Pawlyk, B.S., Bulgakov, O.V., Liu, X., Xu, X., Adamian, M., Sun, X., Khani, S.C., Berson, E.L., Sandberg, M.A., and Li, T. (2010). Replacement gene therapy with a human *RPGRIP1* sequence slows photoreceptor degeneration in a murine model of Leber congenital amaurosis. *Hum. Gene Ther.* 21, 993–1004.
63. Araki, T., Sasaki, Y., and Milbrandt, J. (2004). Increased nuclear NAD biosynthesis and SIRT1 activation prevent axonal degeneration. *Science* 305, 1010–1013.
64. Coleman, M.P., and Freeman, M.R. (2010). Wallerian degeneration, Wld^S, and mmat. *Annu. Rev. Neurosci.* 33, 245–267.
65. Martens, C.R., Denman, B.A., Mazzo, M.R., Armstrong, M.L., Reisdorph, N., McQueen, M.B., Chonchol, M., and Seals, D.R. (2018). Chronic nicotinamide riboside supplementation is well-tolerated and elevates NAD⁺ in healthy middle-aged and older adults. *Nat. Commun.* 9, 1286.
66. Rajman, L., Chwalek, K., and Sinclair, D.A. (2018). Therapeutic potential of NAD-boosting molecules: the in vivo evidence. *Cell Metab.* 27, 529–547.

67. Yang, Y., Mohammed, F.S., Zhang, N., and Sauve, A.A. (2019). Dihydropyridine riboside is a potent NAD⁺ concentration enhancer *in vitro* and *in vivo*. *J. Biol. Chem.* *294*, 9295–9307.
68. Niwa, H., Yamamura, K., and Miyazaki, J. (1991). Efficient selection for high-expression transfectants with a novel eukaryotic vector. *Gene* *108*, 193–199.
69. Zanta-Boussif, M.A., Charrier, S., Brice-Ouzet, A., Martin, S., Opolon, P., Thrasher, A.J., Hope, T.J., and Galy, A. (2009). Validation of a mutated PRE sequence allowing high and sustained transgene expression while abrogating WHV-X protein synthesis: application to the gene therapy of WAS. *Gene Ther.* *16*, 605–619.
70. Hicks, D., and Sahel, J. (1999). The implications of rod-dependent cone survival for basic and clinical research. *Invest. Ophthalmol. Vis. Sci.* *40*, 3071–3074.
71. Campochiaro, P.A., and Mir, T.A. (2018). The mechanism of cone cell death in retinitis pigmentosa. *Prog. Retin. Eye Res.* *62*, 24–37.
72. Gilbert, C., and Foster, A. (2001). Childhood blindness in the context of VISION 2020—the right to sight. *Bull. World Health Organ.* *79*, 227–232.
73. Gilbert, C., and Awan, H. (2003). Blindness in children. *BMJ* *327*, 760–761.
74. Turner, P.V., and Albassam, M.A. (2005). Susceptibility of rats to corneal lesions after injectable anesthesia. *Comp. Med.* *55*, 175–182.
75. Koehn, D., Meyer, K.J., Syed, N.A., and Anderson, M.G. (2015). Ketamine/xylazine-induced corneal damage in mice. *PLoS ONE* *10*, e0132804.
76. Phifer, C.B., and Terry, L.M. (1986). Use of hypothermia for general anesthesia in preweanling rodents. *Physiol. Behav.* *38*, 887–890.